

Stereotomography: a semi-automatic approach for velocity macromodel estimation

G. Lambaré,^{1*} M. Alerini,^{1†} R. Baina² and P. Podvin¹

¹Ecole des Mines de Paris, Centre de Recherche en Géophysique, 35 rue Saint-Honore, 77305 Fontainebleau, and ²OPERA, Pau, France

Received January 2004, revision accepted July 2004

ABSTRACT

Most methods for velocity macromodel estimation require considerable operator input, mainly concerning the regularization and the picking of events in the data set or in the migrated images. For both these aspects, slope tomography methods offer interesting solutions. They consider locally coherent events characterized by their slopes in the data cube. Picking is then much easier and consequently denser than in standard traveltimes tomography. Stereotomography is the latest slope tomography method. In recent years it has been improved significantly, both from an algorithmic point of view and in terms of practical use. Robust and fast procedures are now available for 2D stereotomographic picking and optimization.

Concerning the picking, we propose simple criteria for the selection of relevant data among the automatically picked events. This enables an accurate smooth velocity macromodel to be estimated quite rapidly and with very limited operator intervention. We demonstrate the method using a 2D line extracted from the Oseberg NH8906 data set.

INTRODUCTION

Prestack depth migration remains the best way of imaging the subsurface, in particular in areas of complex geology. This process is, however, very sensitive to the velocity macromodel and therefore great care must be taken at this very important step (Fagin 1998). Since standard approaches based on Dix's formula are not acceptable in complex media, two main types of method remain available: migration-based velocity analysis (MVA) and traveltimes tomography. Tomography is particularly interesting in the case of 3D applications for which MVA is expensive, although traveltimes picking in 3D tomography is a difficult and time-consuming process, requiring significant expertise.

In order to facilitate the picking, a slope tomography method, known as stereotomography, was proposed for es-

timating velocity macromodels from surface reflection data (Billette 1998; Billette and Lambaré 1998). This method requires, at least in principle, much less effort in interpreting the seismic events used for velocity estimation. The efficiency of stereotomography has been demonstrated over several years (Le Bégat, Podvin and Lambaré 2000; Alerini 2002; Alerini *et al.* 2002, 2003a; Chalard *et al.* 2002; Nguyen *et al.* 2002; Billette *et al.* 2003; Gosselet, Le Bégat and Petersen 2003; Lambaré *et al.* 2003a,b).

In recent years, the development of P-P and P-S stereotomography has led to significant improvements in the stereotomographic method (Alerini 2002; Alerini *et al.* 2002, 2003a,b,c; Lambaré *et al.* 2003a), giving a fast, fairly robust, semi-automatic process. These improvements are principally concerned with the control of numerical regularization and the rejection of outliers in the set of automatically picked events. The relevance of the picked events is a crucial point because stereotomographic inversion is based on minimizing a norm cost function, as is the case in most inversion techniques. Regularization is also a difficult problem. It is often tuned by trial and error (Billette *et al.* 2003) using, for

Paper presented at the EAGE/SEG Summer Research Workshop, Trieste, Italy, August/September 2003.

*E-mail: gilles.lambare@geophy.ensmp.fr

†Now at: SINTEF Petroleum Research, Trondheim, Norway.

example, the so-called ‘L-curves’ introduced by Pratt and Chapman (1992).

In this paper, we first give a brief overview of the theoretical and practical aspects of stereotomography. We then present our strategy for semi-automatic application and demonstrate it using the real Oseberg NH8906 data set (Tura, Hanitzsch and Calandra 1997; Thierry *et al.* 1999, 2000; Chauris and Noble 2001).

STEREOTOMOGRAPHY

Slope tomography methods rely on the concept of locally coherent events. A locally coherent event can be described by the positions of the shot and the receiver (s, r), the two-way traveltimes T_{sr} , and the slopes of the event in the common-shot and common-receiver directions (p_s, p_r) (Fig. 1). Stereotomography is based on the idea that a locally coherent event provides information about the velocity macromodel (Billette and Lambaré 1998). Several slope tomography methods have been proposed for recovering the velocity macromodel from a set

of picked events with parameters $[(s, r, p_s, p_r, T_{sr})_{i=1,N}]$ (e.g. Riabinkin 1957; Sword 1987).

Among these methods, stereotomography appears to be the most robust. In this approach, the cost function consists of L_2 -norm misfits for all types of data parameter simultaneously. This allows us to introduce uncertainties for all types of data parameter, and ensures the robustness of the local optimization. Consequently, the pair of ray segments associated with each picked event is optimized jointly with the velocity macromodel itself (Billette and Lambaré 1998; Billette *et al.* 2003). A pair of ray segments is described by a common starting position at depth x , two initial angles, β_s and β_r , and two one-way traveltimes, T_s and T_r , for the rays shot towards the shot and receiver, respectively. The stereotomographic model then consists of the parameters $[(x, \beta_s, \beta_r, T_s, T_r)_{i=1,N}; C_{j=1,M}]$, where C_j denote the parameters describing the velocity macromodel. This joint inversion is performed using a non-linear local optimization. The inverted velocity macromodel is smooth and defined by cardinal cubic B-splines (de Boor 1978). The Fréchet derivatives, with respect to the velocity parameters, are computed by paraxial ray tracing, and second-order continuity

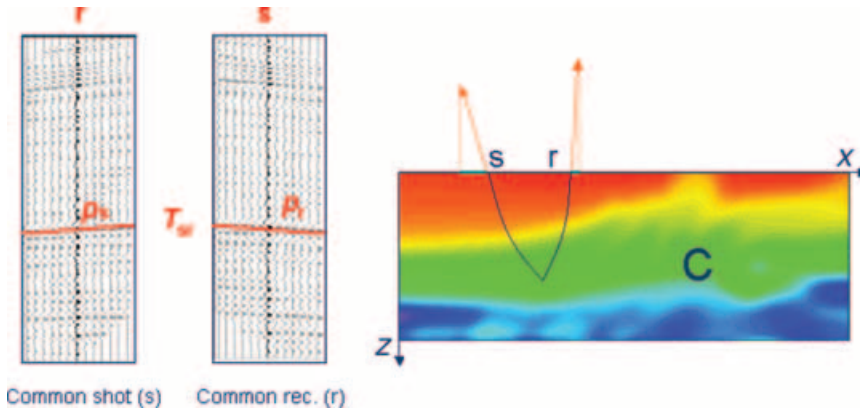


Figure 1 Interpretation of a locally coherent event characterized by its central shot and receiver positions, s and r , its slopes, p_s and p_r , and the traveltimes, T_{sr} . A pair of ray segments (right) can be associated with the event (left) (from Lambaré 2002).

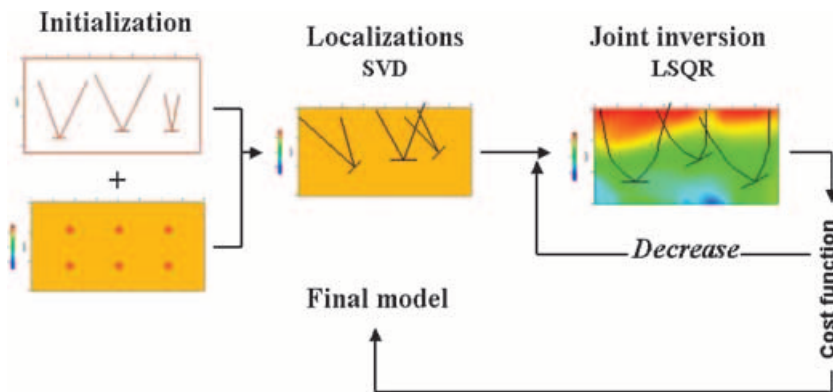


Figure 2 The algorithm for the non-linear stereotomographic optimization (from Le Bégat *et al.* 2000). Initialization consists of first defining an initial set of pairs of ray segments and an initial velocity model. In the localization step, the pairs of ray segments are then optimized fixing the velocity model. Finally, a joint optimization of the pairs of ray segments and of the velocity model is carried out.

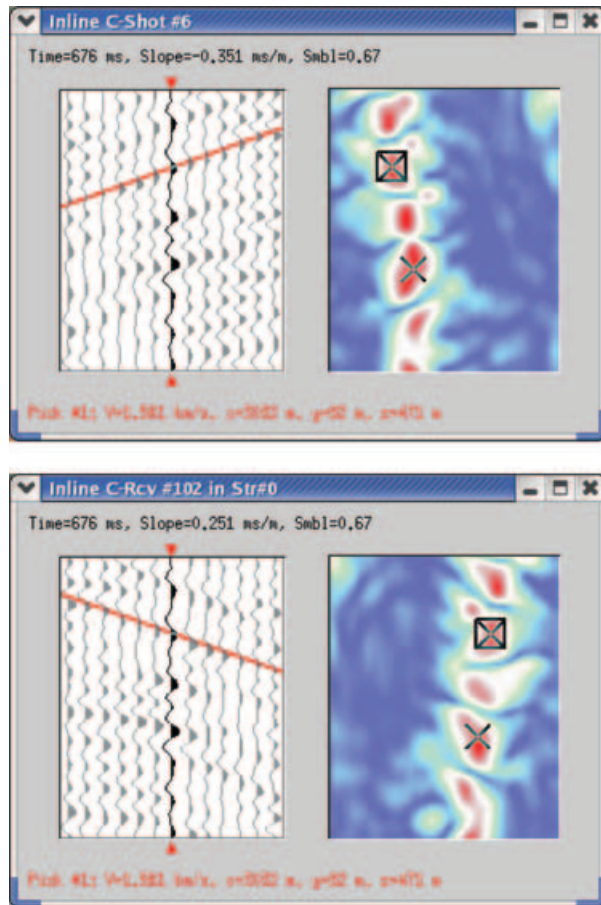


Figure 3 Quality control of the automatic stereotomographic picking. Top: common-shot section. Left: the trace gather centred round the central trace indicated by two small red triangles. Right: the panel shows the envelope of the associated local slant stack of the traces (crosses indicate the automatically picked events). The horizontal dimension is horizontal slope, the vertical dimension is time. An apodizing weight was applied to the traces laterally in order to avoid abrupt truncation artefacts (Billette *et al.* 2003). For both panels, the vertical dimension is time. Bottom: the corresponding common-receiver gather centred on the same central trace. Stereotomographic picking requires picking the same event on the two local slant-stack panels.

of the velocity macromodel is required (Farra and Madariaga 1987). The extension of stereotomography to 3D is straightforward. We simply have to add the lateral dimension for all the types of data and model parameters. For practical application of the method, the important result was to discover that in 3D stereotomography the velocity macromodel can be constrained from a single lateral slope at the surface (at either the shot or receiver point), leading to much easier stereotomographic picking on 3D multistreamer marine acquisitions (Chalard *et al.* 2000, 2002).

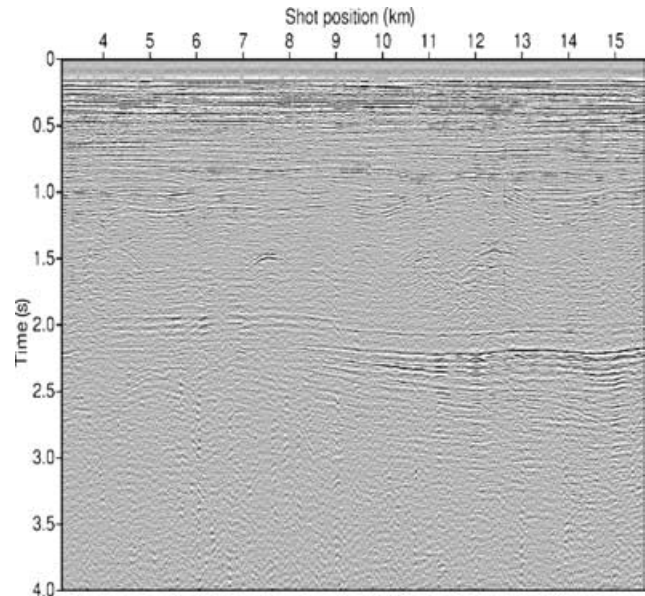


Figure 4 Near-offset section for a 2D line extracted from the Oseberg NH8906 data set.

The stereotomography algorithm consists of the following three steps (Fig. 2):

- 1 Initialization, consisting of building the *a priori* model (pairs of ray segments and velocity model). In practice we use simple starting models, e.g. a homogeneous velocity model and ray segments derived from simple geometrical considerations.
- 2 Localization of the events (i.e. optimization of each pair of ray segments) in the *a priori* velocity model. This is done using a Newton-type non-linear optimization. Since all events can be localized independently, we use singular value decomposition. The localization step leads to an important reduction of the cost function.
- 3 Joint iterative inversion of ray segments and velocity model parameters. This is realized using the LSQR scheme (Paige and Saunders 1982). A regularization term is introduced for the velocity model using Laplacian-type regularization.

The tuning of the LSQR scheme and of the Laplacian regularization can be performed simply (Alerini 2002; Alerini *et al.* 2002, 2003a,b,c; Lambaré *et al.* 2003a,b). For the tuning of the LSQR algorithm we followed the recommendations of Paige and Saunders (1982), while for the Laplacian regularization we used the empirical law given by Wang (1993). Practically a weighting factor was applied to the Laplacian regularization so that the energy of the components of the Fréchet derivatives associated with the Laplacian-type regularization was one-tenth of the energy associated with the misfits on the

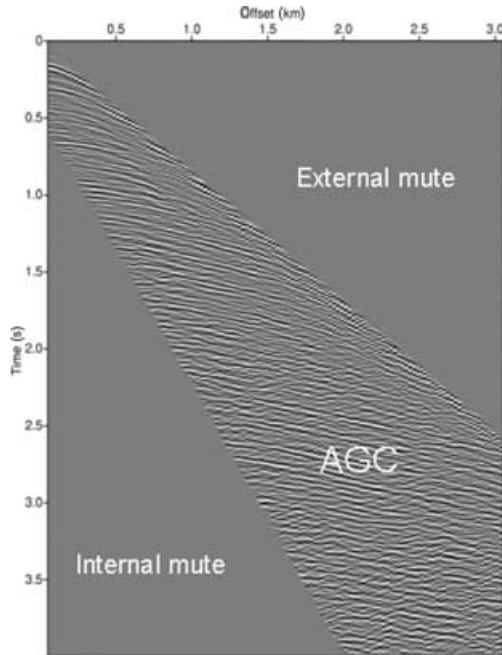


Figure 5 Common-shot gather for the first shot after the preprocessing required by the stereotomographic picking. An automatic gain compensates the natural decay of the amplitude of the reflected arrival along the time axis. Internal and external mutes are used to restrict picking to the data region where stereotomographic information can be used for constraining the velocity model. At short offsets no information is available for the velocity model in the stereotomographic approach, due to the depth–velocity ambiguity.

stereotomographic data parameters. In practice, such criteria can be straightforwardly used as black boxes.

The second crucial point is the picking of relevant events. Stereotomography does not require the events to be tied to interpreted reflectors in depth. Moreover, only local coherence is required and events can be treated as being independent. Consequently, in principle the method allows much denser and much easier picking than standard traveltime tomography (Farra and Madariaga 1988). In practice, an initial set of events can be blindly and automatically picked with the help of local slant-stack panels (Billette *et al.* 2003) (Fig. 3).

Since the least-squares cost function used in inversion is particularly sensitive to outliers in the data, erroneously picked events may have to be eliminated from the database. We propose, and demonstrate on a real data set, a semi-automatic strategy to perform this selection.

The selection of the events can be carried out using various procedures, ranging from an interactive visual check (Alerini *et al.* 2003a,b,c) to an automatic or semi-automatic selection. Among the various criteria that can be used for the selection are:

- The statistical distribution of data parameters (the obvious outliers can be removed from the stereotomographic data set).
- The equivalent model associated with each picked event (Billette *et al.* 2003). Lambaré *et al.* (2003a) used this

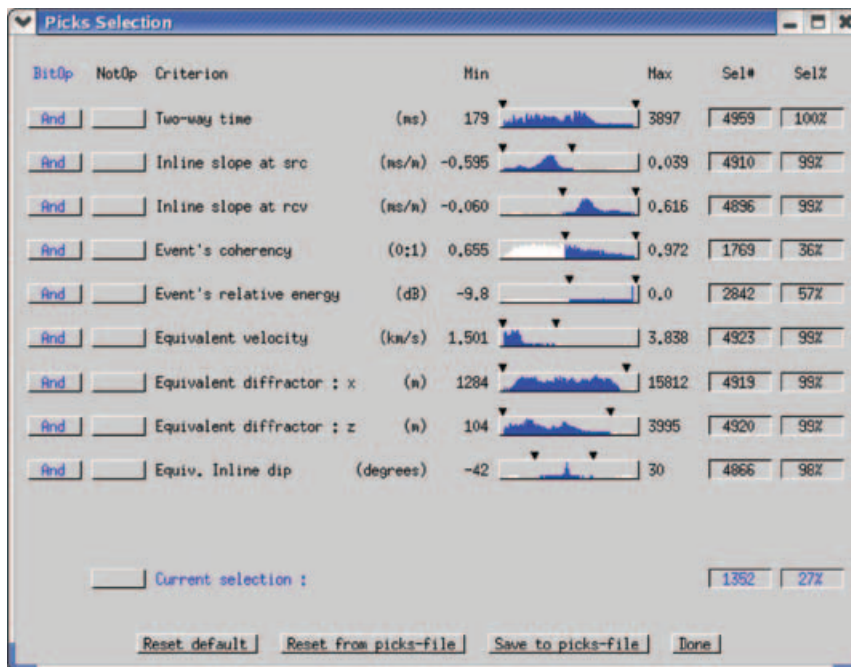
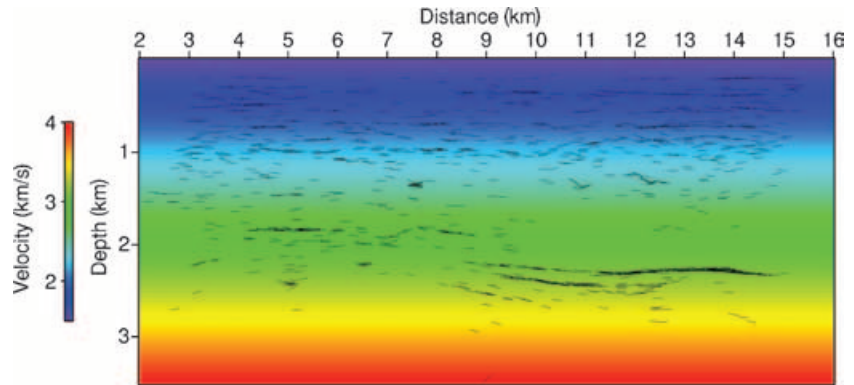


Figure 6 *A priori* selection of stereotomographic events. The selection is made according to various criteria. Each line shows the name of the criterion, its unit and its population distribution between its extreme values. Selection consists of defining new minimum and maximum selection values. The population of selected events is shown in blue, rejected events are in white. At the right, the number of selected events is given and also its percentage with respect to the total number of events. In the present case, outliers have been eliminated because of slope and equivalent mode parameters (Billette *et al.* 2003), and events with the highest energy (57% of the events) and coherence (36% of the events) have been kept. The global selection of events is a superposition of all the individual selections and is given against 'Current selection'; thus 1352 events have been selected.

Figure 7 Initial stereotomographic model, with the dip bars corresponding to the location and dip of the stereotomographic events localized in this initial model. The velocity model consists of a linear increase in velocity with depth.



information to select events according to the stacking velocities obtained by a standard time processing.

- The coherence and energy of the events used systematically.
- The misfits associated with the stereotomographic events after a first run of the stereotomographic inversion.

Of these various criteria, we use those that allow easy automatic or semi-automatic selection of the events; for example, the elimination of the outliers after the automatic picking, or, after some stereotomographic optimization, the selection according to the coherence or the energy, may result in simple interactive selections.

APPLICATION TO A REAL DATA SET (OSEBERG NH8906)

We have chosen a typical 2D marine line extracted from the Oseberg NH8906 data set (Fig. 4). The aim of the present application was to investigate whether a simple strategy could be applied to this real data set, resulting in a semi-automatic approach for stereotomography.

Some simple preprocessing was carried out on these data to improve the quality of the picked events. For the stereotomographic picking, we applied an automatic gain control (AGC) followed by internal and external mutes to the traces. The mutes were introduced in order to avoid the picking of erroneous or uninformative events for stereotomography (e.g. the short offset events). Figure 5 shows a typical shot after this preprocessing step.

The automatic picking was performed every 150 m for common-shot and common-receiver gathers (this was also the half-width of the local slant-stack windows). In addition, clusters of quasi-parallel events differing by less than 200 ms were excluded. After this automatic picking, a further selection of the events was made, with regard to their energy and coherence, and the outliers were eliminated

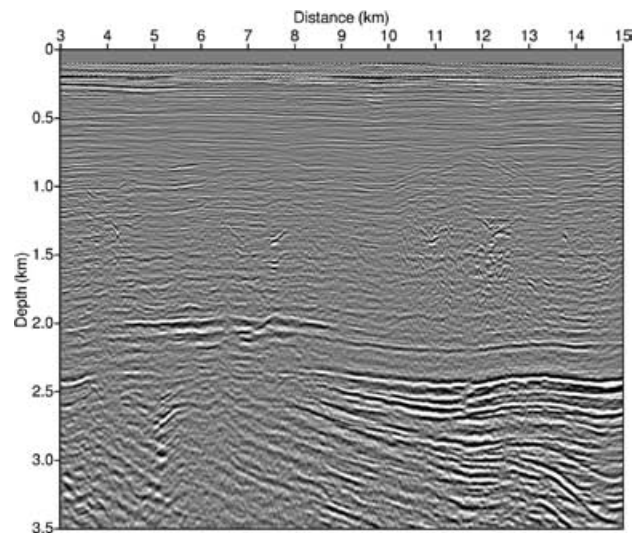


Figure 8 Preserved amplitude migrated image for the initial stereotomographic model.

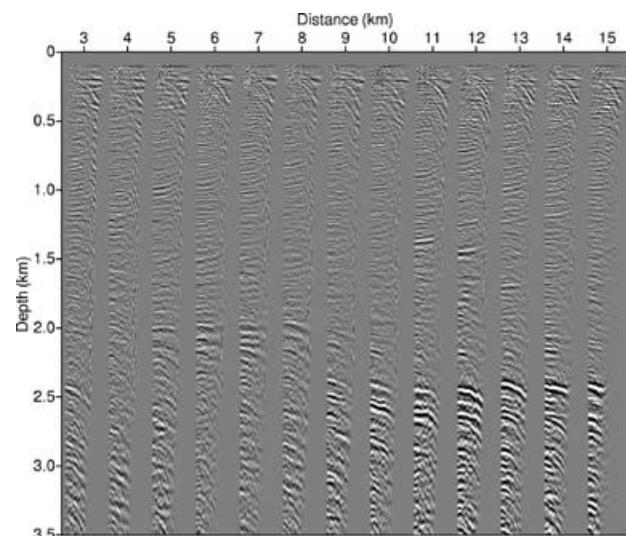


Figure 9 Common-image gathers in the angle domain in the initial stereotomographic model.

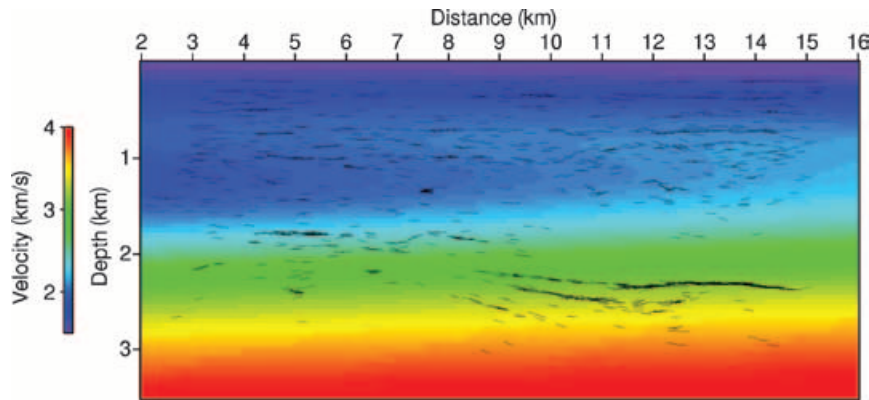


Figure 10 Stereotomographic model after five iterations with the coarse B-spline representation of the velocity model.

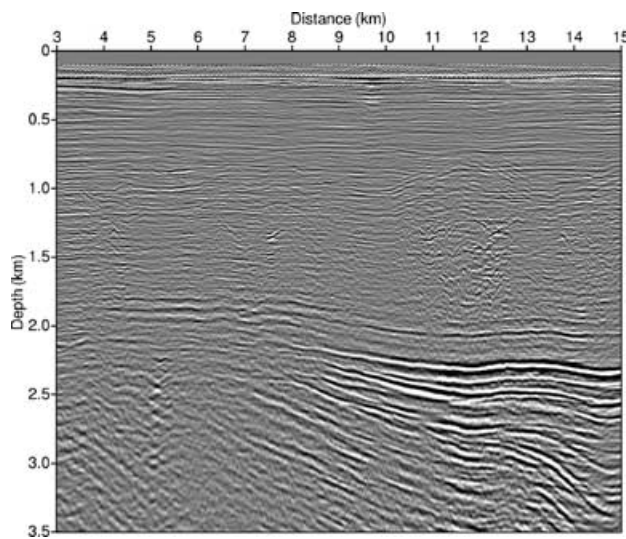


Figure 11 Preserved amplitude migrated image after five iterations with the coarse B-spline representation of the velocity model.

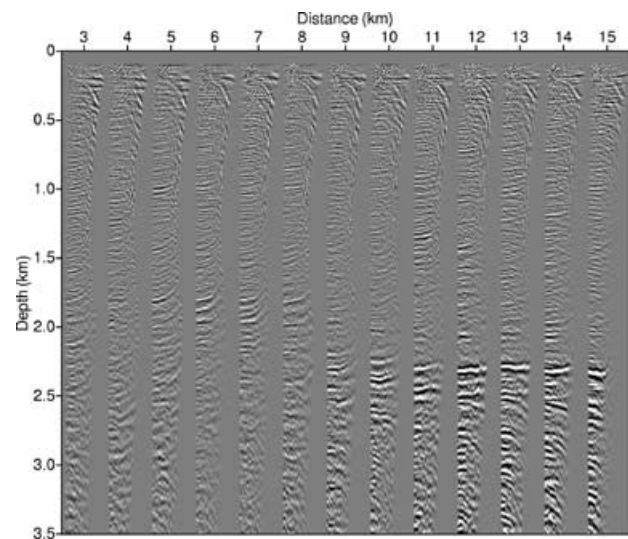


Figure 12 Common-image gathers in the angle domain after five iterations with the coarse B-spline representation of the velocity model.

(Fig. 6). This left 1352 events to be used for the stereotomographic optimization.

For this inversion, we used a multiscale approach. This is also an easy way of regularizing the inversion. The optimization started using a velocity model described by B-splines spaced at intervals of 400 m vertically and 10 km horizontally. The initial model was a constant-velocity-gradient model, shown in Fig. 7 with the dip bars associated with the stereotomographic events after the localization step. The dip bars represent the pairs of ray segments. Each dip bar is located at the inverted reflection/diffraction point position and its slope is the inverted geological slope. Figures 8 and 9 show the associated preserved amplitude migration and common-image gathers in the angle domain, respectively.

For the joint optimization, we initially used a strong Laplacian regularization, i.e. 10 times the empirical weight recom-

mended by Wang (1993). We performed five non-linear iterations. Figure 10 shows the resulting stereotomographic model. Figures 11 and 12 show the associated preserved amplitude migration and common-image gathers in the angle domain, respectively.

At this point the density of the velocity macromodel is increased. The B-splines are now spaced at intervals of 200 m vertically and 625 m horizontally, which should enable the inversion of a less smooth, more realistic model. The weighting of the Laplacian regularization remains the same as before. It is not reduced to the value recommended by Wang (1993), due to the higher level of noise in real data.

Figure 13 shows the resulting stereotomographic model, while Figs 14 and 15 show the associated preserved amplitude migration and common-image gathers in the angle domain,

Figure 13 Stereotomographic model after five iterations with the fine B-spline representation of the velocity model.

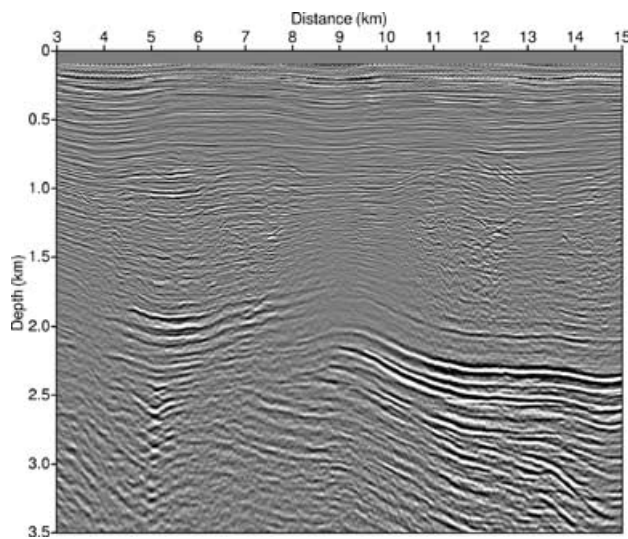
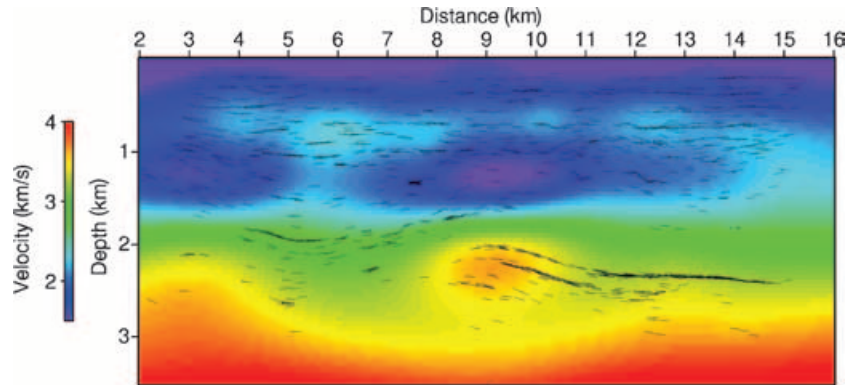


Figure 14 Preserved amplitude migrated image after five iterations with the fine B-spline representation of the velocity model.

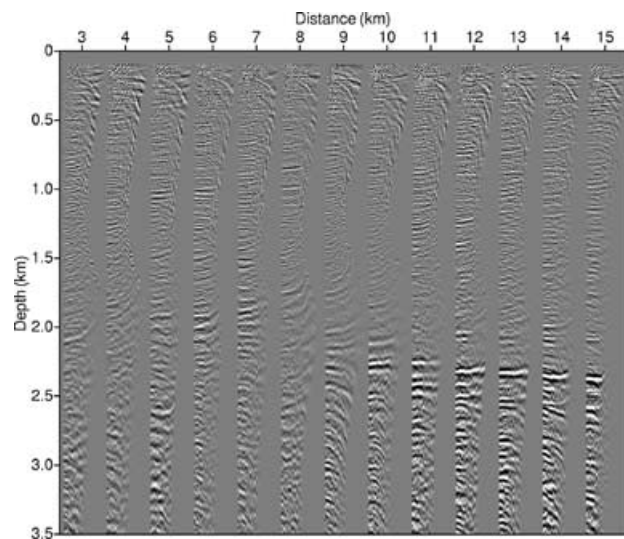


Figure 15 Common-image gathers in the angle domain after five iterations with the fine B-spline representation of the velocity model.

respectively. Lateral structures and also velocity inversions appear in the velocity model. However, reflectors in the migrated image exhibit strong spurious oscillations and the associated common-image gathers are not focused. In fact, the convergence has been altered by erroneous picked events. They have to be identified and removed from the stereotomographic data set.

The first strategy that we investigated was eliminating the outliers in terms of stereotomographic misfit. We decided to eliminate the picked events associated with a normalized squared misfit greater than 100. Some of the eliminated picked events are shown in Fig. 16. They may correspond to some ambiguity in the characterization of the slope of the event.

Figure 17 shows the selected events that are relocated in the final velocity model (Fig. 13). Almost 30% of the events were eliminated, leaving 962 events instead of 1352.

With this new stereotomographic data set, we restarted the stereotomographic inversion from the initial velocity model (Fig. 7). We applied the same multiscale approach but, in this case, 10 non-linear iterations were carried out. Figure 18 shows the resulting stereotomographic model, while Figs 19 and 20 show the associated preserved amplitude migration and common-image gathers in the angle domain, respectively.

The stereotomographic inversion now converges to a much better velocity model in the sense that the common-image gathers are reasonably flattened, and no spurious oscillations appear in the migrated image (except in the left part of the profile, where the result is affected by boundary effects). We still see some significant lateral variations of the velocity model, especially in the shallow part.

In the common-image gathers, we see some small up- and down-going events, which can be associated with the

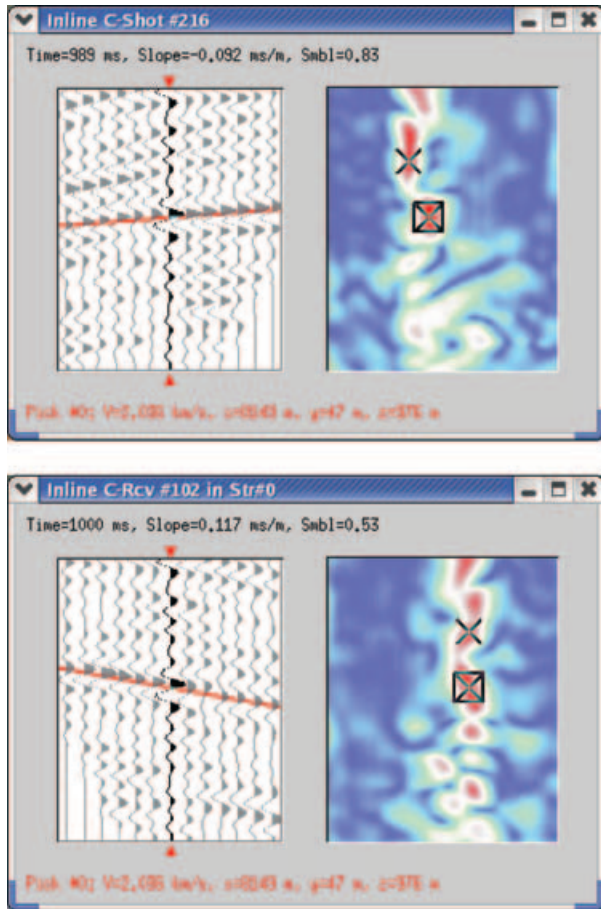


Figure 16 Stereotomographic pick eliminated after the *a posteriori* selection of stereotomographic events. Top: the common-shot panel; bottom: the common-receiver panel. The common-receiver trace gather in the left panel shows an ambiguity in the slope of the event, due to a slight interference between two events.

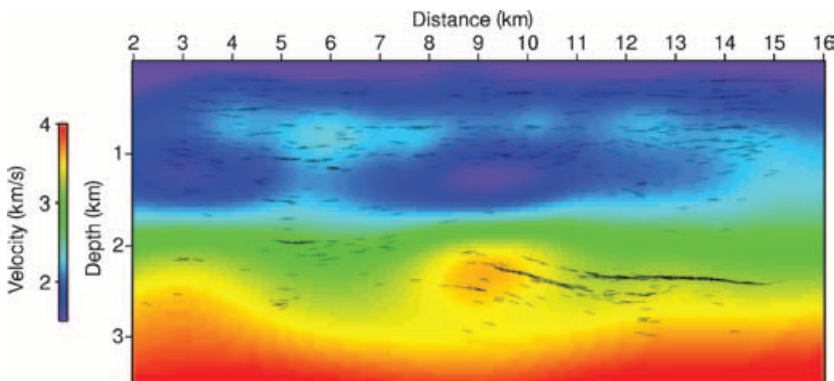


Figure 17 Stereotomographic model after five iterations with the fine B-spline representation of the velocity model, and after *a posteriori* selection of events.

remaining water-bottom multiples (a frequent problem in North Sea data sets). When they are picked, stereotomography provides an average velocity model. An *a posteriori* selection of events, using the slope in the common-image gathers, could be an opportunity for removing them from the stereotomographic optimization. This approach requires further investigation, and may result in an interesting alternative to stereotomographic picking in the depth-migrated domain (Chauris *et al.* 2002a,b; Nguyen *et al.* 2002).

Another possibility for reducing the effect of outliers in the stereotomographic data set could be to increase the number of stereotomographic events. We tested this possibility with an automatic picking, carried out every 50 m in the common-shot and common-receiver directions (rather than every 150 m as previously). Figure 21 shows the resulting stereotomographic model, while Figs 22 and 23 show the associated preserved amplitude migration and common-image gathers in the angle domain, respectively. The same multiscale optimization as previously was used. An interactive *a priori* selection of the events (Fig. 6) was used but no *a posteriori* selection using stereotomographic misfit was introduced. A total of 13 620 stereotomographic events were used. The result obtained is certainly the best in view of the flatness of common-image gathers and of the quality of the migrated image. It demonstrates that increasing the number of stereotomographic data stabilizes the stereotomographic optimization. The computing time required for stereotomographic optimization depends linearly on the number of data, and consequently increasing the number of data is quite acceptable. In any case, the *a posteriori* selection of the events is very simple, and we advise that it is carried out for security.

Figure 18 Stereotomographic model after 10 iterations with the fine B-spline representation of the velocity model, and after *a posteriori* selection of events.

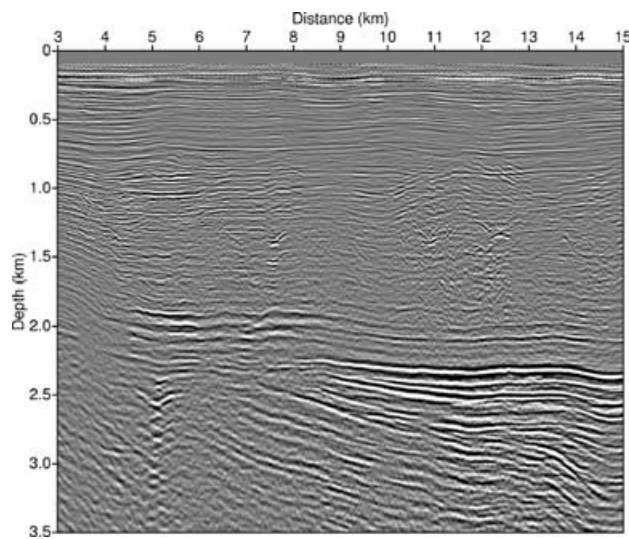
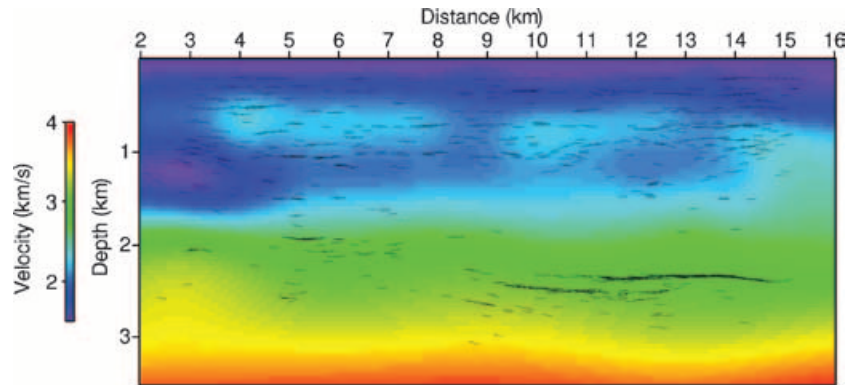


Figure 19 Preserved amplitude migrated image after 10 iterations with the fine B-spline representation of the velocity model, and after *a posteriori* selection of events.

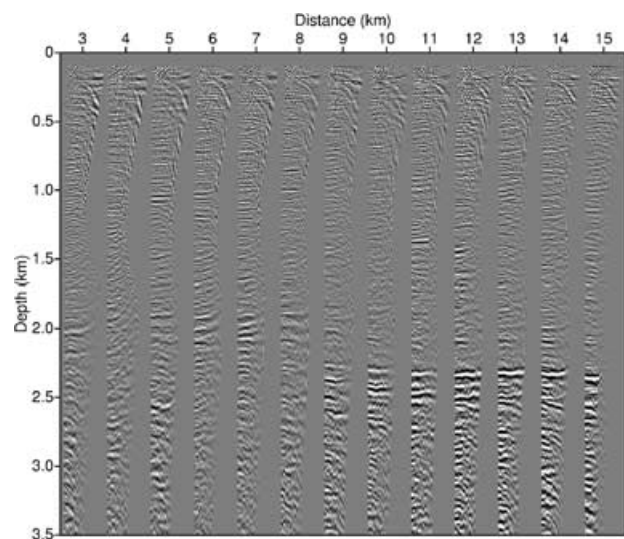


Figure 20 Common-image gathers in the angle domain after 10 iterations with the fine B-spline representation of the velocity model, and after *a posteriori* selection of events.

CONCLUSION

Stereotomography has now been carried out on several data sets, and appears to be an accurate and practical approach to estimating velocity macromodels from seismic reflection data. We have proposed simple and robust strategies both for the selection of stereotomographic events after the automatic picking and for the regularization of the stereotomographic optimization itself. The resulting strategy appears to be quite robust and to enable a semi-automatic estimation of velocity macromodels for depth imaging to be made. However, the real data set, Oseberg NH8906, which has been processed here, cannot be seen as a complex case. The applicability of stereotomography to complex models (with strong lateral variations in the velocity model) still needs to be investigated.

Significant improvements can still be made. As far as the picking is concerned, the selection criteria both before and after the stereotomographic inversion must be improved. For the stereotomographic optimization itself, more improvements should be made to the algorithm. For example, the possibility of removing picked events during the optimization scheme should be introduced. The introduction of an L_1 -cost function should also be tested for improving the robustness of the inversion. The extension to 3D (Chalard *et al.* 2002) will benefit from this work, leading to a fast and robust tool.

ACKNOWLEDGEMENTS

We thank Norsk Hydro for the real data set, and the sponsors of the DIG consortium for partly funding this work. We also thank Adam Gosselet (Ecole des Mines), Sylvain Nguyen

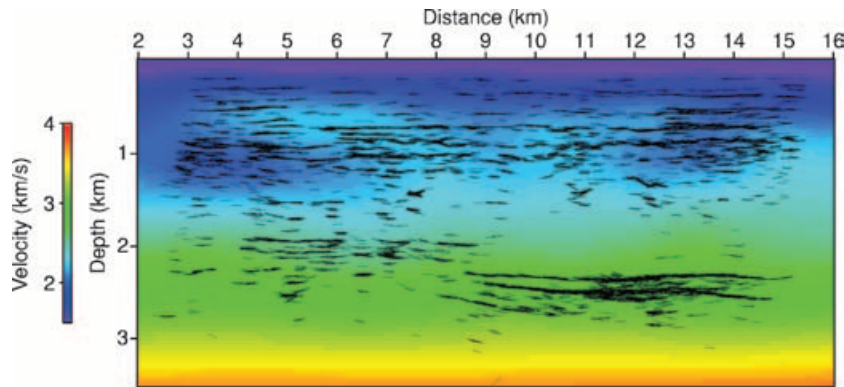


Figure 21 Stereotomographic model after five iterations with the fine B-spline representation of the velocity model, and a dense stereotomographic picking.

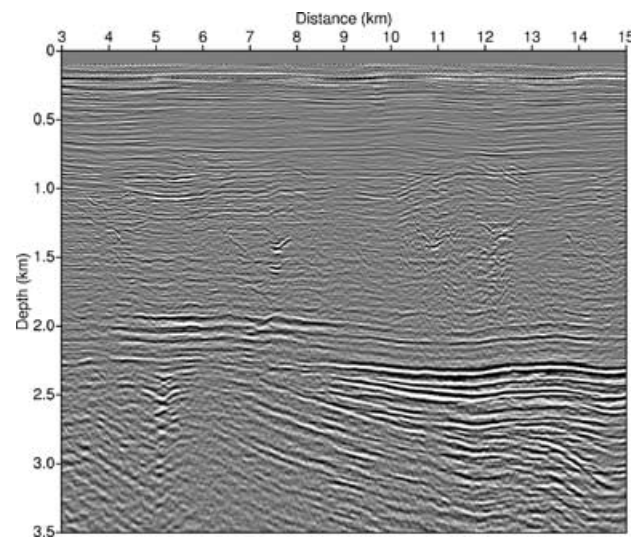


Figure 22 Preserved amplitude migrated image after five iterations with the fine B-spline representation of the velocity model, and a dense stereotomographic picking.

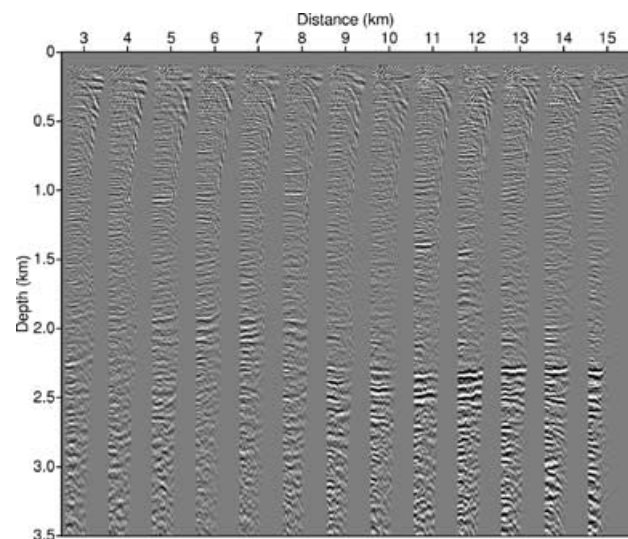


Figure 23 Common-image gathers in the angle domain after five iterations with the fine B-spline representation of the velocity model, and a dense stereotomographic picking.

(Ecole des Mines), Evgeny Landa (OPERA) and Benoit Lavaux (OPERA) for fruitful discussions. We are grateful to Robert Ferguson and to an anonymous reviewer for their help in improving the manuscript.

REFERENCES

- Alerini M. 2002. *Imagerie sismique en profondeur de données OBC via la théorie des rais en milieu isotrope*. PhD thesis, Ecole des Mines de Paris.
- Alerini M., Lambaré G., Baina R. and Podvin P. 2003a. Stereotomography: a fast approach for velocity macromodel estimation. EAGE/SEG Summer Research Workshop, Trieste, Expanded Abstracts, T28.
- Alerini M., Lambaré G., Podvin P. and Le Béat S. 2003b. Stereotomography: extension and application to converted waves. EAGE/SEG Summer Research Workshop, Trieste, Expanded Abstracts, T31.
- Alerini M., Lambaré G., Podvin P. and Le Béat S. 2003c. Depth imaging of the 2D-4C OBC Mahogany dataset: application of PP-PS Stereotomography. 73rd SEG meeting, Dallas, USA, Expanded Abstracts, 850-853.
- Alerini M., Le Béat S., Lambaré G. and Baina R. 2002. 2D P-P and P-S stereotomography of a multi-component dataset. 72nd SEG meeting, Salt Lake City, USA, Expanded Abstracts, 838-841.
- Billette F. 1998. *Estimation de macro-modèles de vitesse en sismique réflexion par stéréotomographie*. PhD thesis, University Paris VII.
- Billette F. and Lambaré G. 1998. Velocity macromodel estimation from seismic reflection data by Stereotomography. *Geophysical Journal International* 135, 671-680.
- Billette F., Le Béat S., Podvin P. and Lambaré G. 2003. Practical aspects and applications of 2D Stereotomography. *Geophysics* 67, 1213-1224.
- Boor C. 1978. *A Practical Guide to Splines*. Springer-Verlag, Inc.

- Chalard E., Podvin P., Lambaré G. and Audebert F. 2000. Estimation of velocity macromodels by 3D Stereotomography. 70th SEG meeting, Calgary, Canada, Expanded Abstracts, 2257–2260.
- Chalard E., Podvin P., Le Bégat S., Berthet P. and David B. 2002. 3D stereotomographic inversion on a real dataset. 72nd SEG meeting, Salt Lake City, USA, Expanded Abstracts, 946–948.
- Chauris H. and Noble M. 2001. Two-dimensional velocity macro model estimation from seismic reflection data by local differential semblance optimisation: application to synthetic and real data sets. *Geophysical Journal International* **144**, 14–26.
- Chauris H., Noble M., Lambaré G. and Podvin P. 2002a. Migration velocity analysis from locally coherent events in 2-D laterally heterogeneous media, Part I: Theoretical aspects. *Geophysics* **67**, 1202–1212.
- Chauris H., Noble M., Lambaré G. and Podvin P. 2002b. Migration velocity analysis from locally coherent events in 2-D laterally heterogeneous media, Part II: Applications on synthetic and real data. *Geophysics* **67**, 1213–1224.
- Fagin S. 1998. *Model-based Depth Imaging*. Society of Exploration Geophysicists.
- Farra V. and Madariaga R. 1987. Seismic waveform modeling in heterogeneous media by ray perturbation theory. *Journal of Geophysical Research* **92**, 2697–2712.
- Farra V. and Madariaga R. 1988. Non-linear reflection tomography. *Geophysical Journal* **95**, 135–147.
- Gosset A., Le Bégat S. and Petersen S. 2003. 2D walk-away transmission Stereotomography. 73rd SEG meeting, Dallas, USA, Expanded Abstracts, 678–681.
- Lambaré G. 2002. The use of locally coherent events in depth processing: a state of the art. 72nd SEG meeting, Salt Lake City, USA, Expanded Abstracts, 2261–2264.
- Lambaré G., Boëlle J.-L. and Alerini M. 2003a. P-P and P-S Stereotomography: an application to a 2D-OBC-4C real dataset. 73rd SEG meeting, Dallas, USA, Expanded Abstracts, 809–812.
- Lambaré G., Alerini M., Baina R. and Podvin P. 2003b. Stereotomography: a fast approach for velocity macromodel estimation. 73rd SEG meeting, Dallas, USA, Expanded Abstracts, 2076–2079.
- Le Bégat S., Podvin P. and Lambaré G. 2000. Application of 2-D stereotomography to marine seismic reflection data. 70th SEG meeting, Calgary, Canada, Expanded Abstracts, 2142–2145.
- Nguyen S., Baina R., Noble M. and Thierry P. 2002. Tomography picking in the depth domain using migration of attributes. 72nd SEG meeting, Salt Lake City, USA, Expanded Abstracts, 1140–1143.
- Paige C. and Saunders M.A. 1982. LSQR: an algorithm for sparse linear equations and least-squares problems. *ACM Transactions on Mathematical Software* **8**, 43–71.
- Pratt R.G. and Chapman C.H. 1992. Traveltime tomography in anisotropic media. II. Application. *Geophysical Journal International* **109**, 20–37.
- Riabinkin L.A. 1957. Fundamentals of resolving power of Controlled Directional Reception (CDR) of seismic waves. In: *Slant Stack Processing*, pp. 36–60. Geophysics Reprint Series Vol. 14, 1991. Society of Exploration Geophysicists. (Translated and paraphrased from *Prikladnaya* **16**, 3–36.)
- Sword S. 1987. *Tomographic determination of interval velocities from reflection seismic data: The method of controlled directional reception*. PhD thesis, Stanford University.
- Thierry P., Jousset P., Baina R., Ribodetti A. and Billette F. 2000. 3-D preserved amplitude processing sequence in a real case. 70th SEG meeting, Calgary, Canada, Expanded Abstracts, 239–242.
- Thierry P., Lambaré G., Podvin P. and Noble M. 1999. 3-D preserved amplitude prestack depth migration on a workstation. *Geophysics* **64**, 222–229.
- Tura A., Hanitzsch C. and Calandra H. 1997. 3-D AVO migration/inversion of field data. *Journal of Seismic Exploration* **6**, 117–125. (Special Issue on Amplitude Preserving Seismic Reflection Imaging.)
- Wang B. 1993. *Improvement of seismic travel-time inversion methods and application to observed data*. PhD thesis, Purdue University.